Magazine of Concrete Research, 1999, **51**, No. 5, October, 325–339

Long-term performance of high-stiffness repairs in highway structures

P. S. Mangat* and F. J. O'Flaherty*

Sheffield Hallam University

This paper presents the results of field monitoring of repair patches in two reinforced concrete highway bridges, Lawns Lane Bridge on the M1 and Gunthorpe Bridge across the River Trent. The repairs were applied by spraying (guniting) repair materials to compression members of the bridges. The structural members were unpropped during repair and throughout the 60 week monitoring period. The strains in the repair patches were monitored with vibrating-wire gauges. Four different repair materials were investigated whose elastic modulus was greater than that of the substrate concrete ($E_{rm} > E_{sub}$). The results show that efficient repairs are achieved with $E_{rm} > E_{sub}$, the optimum relationship being $E_{rm} > 1{\cdot}3E_{sub}$. This enables the repair material to shed a significant proportion of its shrinkage strain to the substrate, thereby reducing restrained-shrinkage tension. It also enables the repair to attract externally applied load from the substrate in the long term. The effect of creep and shrinkage on the performance of the repair patch is also determined. Overall, the results show that current repair standards have limitations with respect to repair material specifications.

KEYWORDS: concrete repair; elastic modulus; structural interaction

Introduction

Current standards for repair material specifications (e.g. Department of Transport[1]) do not take into account in any significant quantitative manner the mismatch in basic material properties such as elastic modulus, shrinkage and creep, and particularly their effect on long-term performance and composite action of the repair patch with the substrate. Emphasis is normally given to short-term properties such as the 28 day strength, bond strength and early-age shrinkage. These properties, although important in their own right, do not give a reliable indication of the long-term performance of the repair and the efficiency of its composite action with the substrate.

Studies show that compatibility between the repair material and substrate concrete with respect to volume change (shrinkage and creep) is important for prevention of cracking.[2,3] Commercially available repair materials, however, are generally prone to substantial shrinkage strains despite claims often made by manufacturers about some products being shrinkage-compensated![4,5] Many commercial repair materials are based on polymer latex formulations and are prone to relatively high creep.[5,6] Such materials display stress–strain relationships which develop excessive deformations at higher levels of stress, which are incompatible with the deformation sustained by substrate concretes.[5,6] The composite action of such materials with the substrate will be inefficient.

The compatibility between the repair material and substrate concrete is affected by dimensional deformation along with physical, chemical and electrochemical properties.[7] Dimensional compatibility is responsible for structural interaction and crack prevention.[2,3] The material properties responsible for dimensional compatibility are shrinkage, thermal expansion, creep and modulus of elasticity. The properties of repair systems, however, change with time.[3–5] It has been recommended[7] that the modulus of elasticity of a repair material should lie within the range ± 10 N/mm^2 of the substrate concrete. The findings of the authors' research presented in this paper and elsewhere contradict

* School of Construction, Sheffield Hallam University, UK.

(MCR 739) Paper received 19 November 1998; last revised 1 April 1999; accepted 27 May 1999.

this recommendation—in particular, as this recommendation permits the use of lower-modulus repairs relative to the substrate. It has also been recommended that good resistance to cracking should be achieved by selecting repair materials of low drying shrinkage, thermal expansion and elastic modulus whereas the tensile strength and creep should be as high as possible.[3] The negative impact of these recommendations on the load-sharing capability of repairs is verified in this paper and elsewhere.[8] It has also been stated that the functions performed by a repair will vary from one situation to another.[9] The two principal functions are structural (stress carrying) and cosmetic (restoration of appearance). The properties required of a material to satisfy structural or cosmetic needs are quite different and may in some instances be completely opposite. The problem of the choice of suitable properties is not solved by seeking those closest to the values of the substrate concrete.[10]

It is generally recognized that the restraint provided by the substrate concrete (and the steel reinforcement) to the free shrinkage of the repair patch can cause tensile cracking. However, there is no information available in the current literature about the optimal relationships between repair and substrate properties which allow effective redistribution of repair material shrinkage into the substrate, thereby reducing restrained-shrinkage tension. Similarly, there is no knowledge about the capacity of repair patches to attract externally applied loads from a substrate of structural members. The optimal relationships between material properties (repair and substrate systems) which are required to provide effective composite action need to be quantified. The research reported in this paper identifies the key parameters and quantifies their relationships to provide effective stress redistribution during the shrinkage and external-load-transfer stages of the repair patch.

This paper presents part of a wide-ranging research project concerned with the long-term performance of repairs in highway bridges. Structural members of three bridge structures were repaired and instrumented for long-term monitoring. Two categories of repair materials with $E_{rm} > E_{sub}$ or $E_{rm} < E_{sub}$ were investigated. Most repair materials were commercially manufactured products. Repairs were applied either by hand, by spraying or by placing flowing materials under a pressure head. Both propped and unpropped members of the bridge structures were subjected to repair. This paper is focused on spray-applied repairs to unpropped bridge members using materials with $E_{rm} > E_{sub}$.

Experimental

Highway bridges repaired and monitored

In situ sprayed-concrete repairs were carried out on typical structural members of two highway bridges which were deteriorating owing to reinforcement corrosion. The two bridges were Lawns Lane Bridge, near Wakefield in West Yorkshire, carrying part of the M1 south of junction 42, and Gunthorpe Bridge, carrying the A6097, in Nottinghamshire. Each structure was maintained in an unpropped state during the repair operation. Lawns Lane Bridge is a three-span reinforced concrete bridge which carries a part of the M1 between junctions 41 and 42. It was built in the mid-1960s and consists of *in situ* deck panels supported by prestressed beams, all of which are carried by reinforced concrete piers and abutments. Gunthorpe Bridge is a three-span reinforced concrete arch bridge spanning the River Trent at Gunthorpe, Nottinghamshire. It was built in 1927 to replace an old iron toll bridge owing to an increase in the heavy traffic using the bridge. The central arch in the bridge spans 38·1 m while the two side arches span 30·9 m. Each arch contains four ribs.

Location and strain monitoring of repair patches

Five repair materials were applied by spraying (guniting) to the piers and abutment of Lawns Lane Bridge (Fig. 1). Three of these repair materials (materials L2, L3 and L4), which had an elastic modulus E_{rm} greater than the elastic modulus of the substrate concrete E_{sub}, are considered in this paper. Material L2 was applied on the east face of the north-west pier (Fig. 1(a)). Repair patches of materials L3 and L4 were applied on the north abutment (Fig. 1(b)).

Three repair materials, G1, G2 and G3, were applied by spraying at Gunthorpe Bridge. Only one material (material G1), which had an elastic modulus greater than that of the substrate concrete, is considered in this paper. Fig. 2 shows the location of repair patches on the south abutment at Gunthorpe Bridge. The area of each repair patch was approximately 1·8 m × 2·3 m with a depth of approximately 140 mm.

The piers and abutments at Lawns Lane and Gunthorpe Bridge were reinforced with horizontal and vertical reinforcement. At Lawns Lane both the vertical and the horizontal reinforcement comprised 20 mm dia. high yield bars at 300 mm spacing. The vertical reinforcement at Gunthorpe Bridge was 20 mm dia. plain bars at 325 mm spacing; the horizontal steel was 6 mm dia. links at 300 mm spacing. The deteriorated concrete was cut to approximately 25 mm behind the reinforcement bars to fully expose the steel before repair at both Lawns Lane and Gunthorpe Bridges. The repair patch surrounded the reinforcement bars and developed full bond with them. The thickness of the abutment at Gunthorpe Bridge exceeded 4·3 m and the overall dimensions in elevation were 12·1 × 4·1 m. In comparison, the repair patch dimensions were 1·8 × 2·3 m with 140 mm thickness. Consequently, the size of the repair relative to the substrate was very small and, therefore, the restraint provided by the substrate was high. In the case of Lawns Lane Bridge, the dimensions of the repair patches relative to the substrate were more significant.

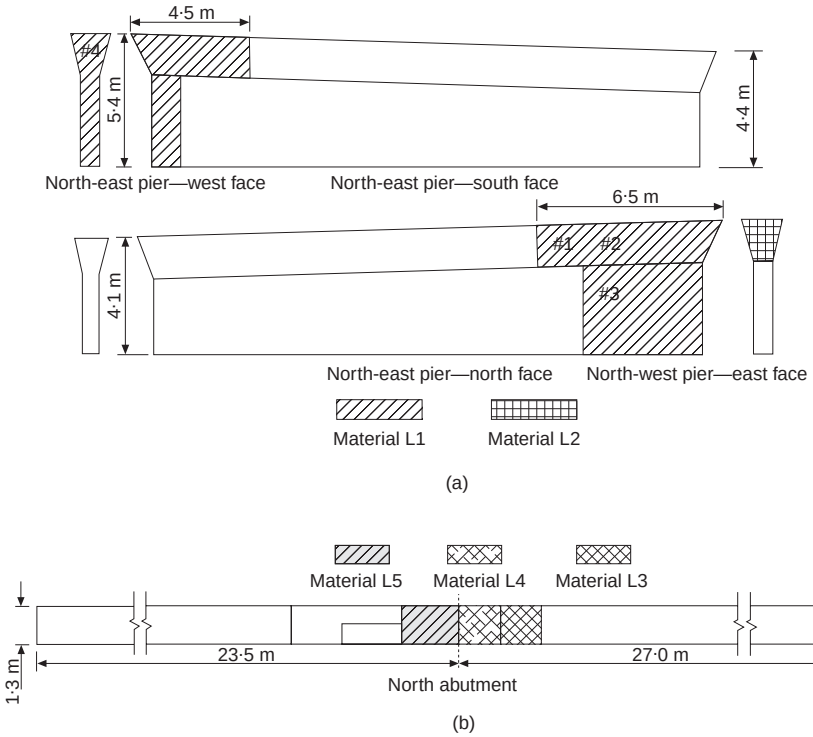

Fig. 1. Location of repair patches at Lawns Lane Bridge: (a) elevation of north-east and west piers; (b) elevation of north abutment (not to scale)

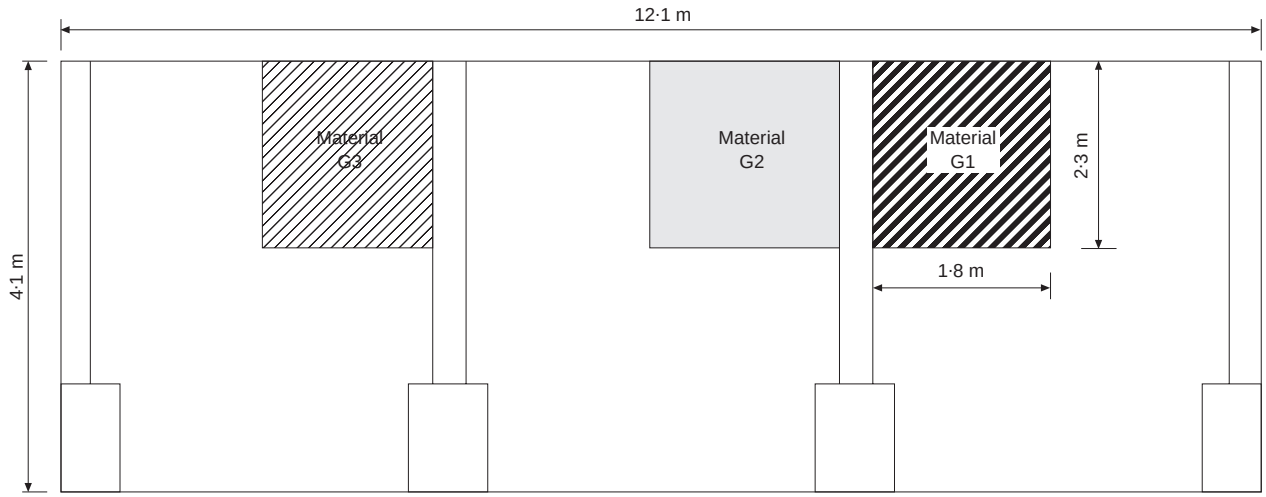

Fig. 2. Location of repair patches at Gunthorpe Bridge (south abutment) (not to scale)

Vibrating-wire strain gauges (gauge length 140 mm) were located in the repair patches at both Lawns Lane and Gunthorpe bridges to monitor the long-term strain distribution within the different phases of a repair patch (substrate interface, steel reinforcement and repair material). The gauge locations in a typical repair patch are shown in Fig. 3. Three gauges were positioned in each repair—one attached to the cut-back surface of the substrate at the interface with the repair (labelled 'subs' in Fig. 3), one welded to the steel reinforcement (labelled 'steel') and one embedded within the body of the repair material at equal distances from adjacent reinforcing bars (labelled 'emb' in Fig. 3).

The long-term redistribution of strain in the repair patches was monitored by means of vibrating-wire gauges, which operate on the principle that an increase in the tensile strain causes a higher frequency of the vibrating wire. The change in strain is given by the expression

$$\delta\varepsilon = k(f_1^2 - f_2^2) \tag{1}$$

where $\delta\varepsilon$ is the change in strain, k is the gauge con-

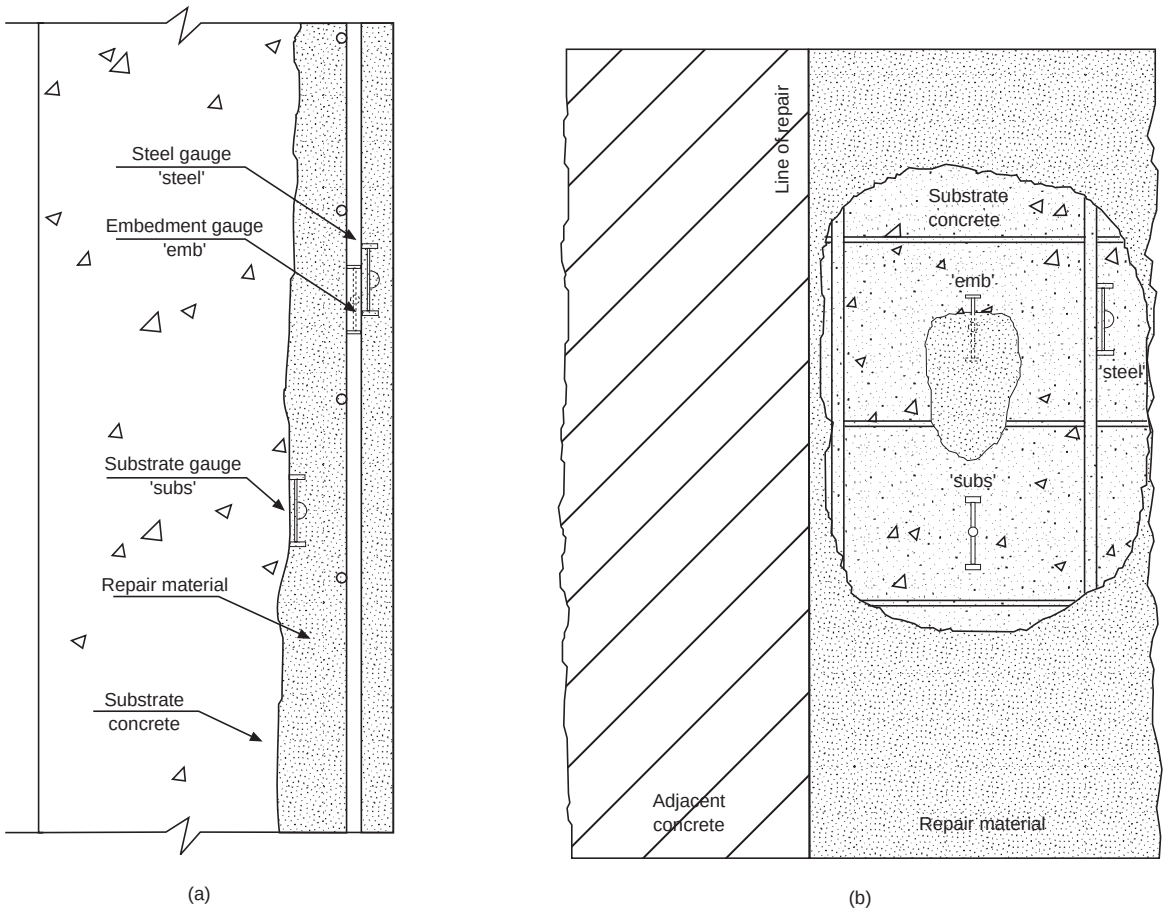

Fig. 3. Position of vibrating-wire strain gauges within a typical repair patch: (a) elevation of a repair; (b) section through a repair

stant (3×10^{-3}), f_1 is the datum frequency (in hertz) and f_2 is the frequency after the strain change (in hertz). (A positive sign indicates a compressive strain, i.e. shortening; a negative sign indicates a tensile strain, i.e. elongation.)

The strain monitoring will continue for many years. Data for the first 60 weeks of monitoring are presented in this paper. An update providing more long-term data will be published in due course.

Repair materials

The four repair materials considered in this paper (L2, L3, L4 and G1) are commercially available and are supplied as single-component systems requiring only the addition of clean water on site. The basic properties of the materials, such as elastic modulus, shrinkage and creep, were determined in the laboratory. The elastic modulus was determined at 28 days' age according to BS 1881: Part 121.[11] The compressive strength of the repair materials was determined using $100 \times 100 \times 100$ mm cubes according to BS 1881: Part 116.[12] The shrinkage and creep of the repair materials were determined on $100 \times 100 \times 500$ mm prisms. The test procedures are given in detail elsewhere.[4,5] Shrinkage specimens were demoulded at 24 h after casting and then exposed to an environment of 20°C, 55% relative humidity (RH) throughout the shrinkage monitoring period. The prism specimens for creep tests were cured in water (at 20°C) for 28 days after casting. They were then loaded in standard creep rigs[4,5] maintaining a constant compressive load equivalent to a stress/28 day cube strength ratio of 30%. Typical properties of the repair materials and the substrate concrete are given in Tables 1 and 2. The substrate concrete properties were determined according to BS 1881: Part 121 using cores of 100 mm dia. $\times$ 180 mm depth, which were drilled from the bridge elements.

Material L2 is a polymer-modified repair mortar designed for machine application using the dry spray

Table 1. Properties of repair materials and substrate concrete

Material	Elastic modulus: kN/mm^2	Compressive strength: N/mm^2	Bridge
Substrate	23·8	42	
L2	30·3	60	Lawns
L3	27·4	35	Lane
L4	29·1	60	
Substrate	28·1	45	Gunthorpe
G1	31·1	60	

Table 2. Relative stiffness, free shrinkage and creep properties

Material	E_{rm}/E_{sub}	Shrinkage: microstrain*	Creep: microstrain†	Bridge
L2	1·27	325	Not available	
L3	1·15	710	748	Lawns
L4	1·22	782	510	Lane
G1	1·10	751	421	Gunthorpe

* Free shrinkage strain at 100 days, stored at 20°C, 55% RH.
† Compression creep, stress/strength 30%, 70 days under load.

process. It is particularly suitable on large repairs to reinforced concrete structures. The 28 day compressive strength is 60 N/mm^2, the density is approximately 2100 kg/m^3 and the modulus of elasticity is 30·3 kN/mm^2.

Material L3 is a repair mortar for general-purpose use. It can be applied by the wet or dry spray process. The material is based on Portland cement, graded aggregates, special fillers and chemical additives. At a typical water/cement ratio of 0·18, the 28 day compressive strength is 35 N/mm^2, the fresh density is 1850 kg/m^3 and the elastic modulus is 27·4 kN/mm^2.

Material L4 is a factory-blended material for dry spray application. It contains Portland cement, silica sand and admixtures including plastic fibres. The maximum aggregate size of the sand is 5 mm. The 28 day compressive strength of the sprayed material at a water/cement ratio of 0·35 is 60 N/mm^2. The elastic modulus is 29·1 kN/mm^2.

Material G1 consists of rapid-hardening Portland cement (minimum content 400 kg/m^3), 5 mm-maximum-size graded limestone aggregate, silica fume and a copolymer. The 28 day compressive strength is 60 N/mm^2, the dry density is 2250 kg/m^3 and the elastic modulus is 31·1 kN/mm^2.

Materials L2, L3 and L4 did not comply with the current standard for repair materials according to the specification of the Highways Agency, BD 27/86.[1] Material G1 conformed to the standard.

Results and discussion

Actual distribution of strain

The distribution of strain with time in the different phases of a repair patch is shown in Figs 4–7 for repair materials L2, L3, L4 (Lawns Lane Bridge) and G1 (Gunthorpe Bridge). Datum readings of strain were taken 24 h after the application of the repair (week 0 on the graphs) and the data are plotted at weekly intervals. Figs 4–7 show that the strain in the substrate concrete ('subs') increases rapidly during approximately the first 11 weeks after the application of the repair. From week 11 to week 25 (approximately), the strain in the substrate remains relatively constant. After

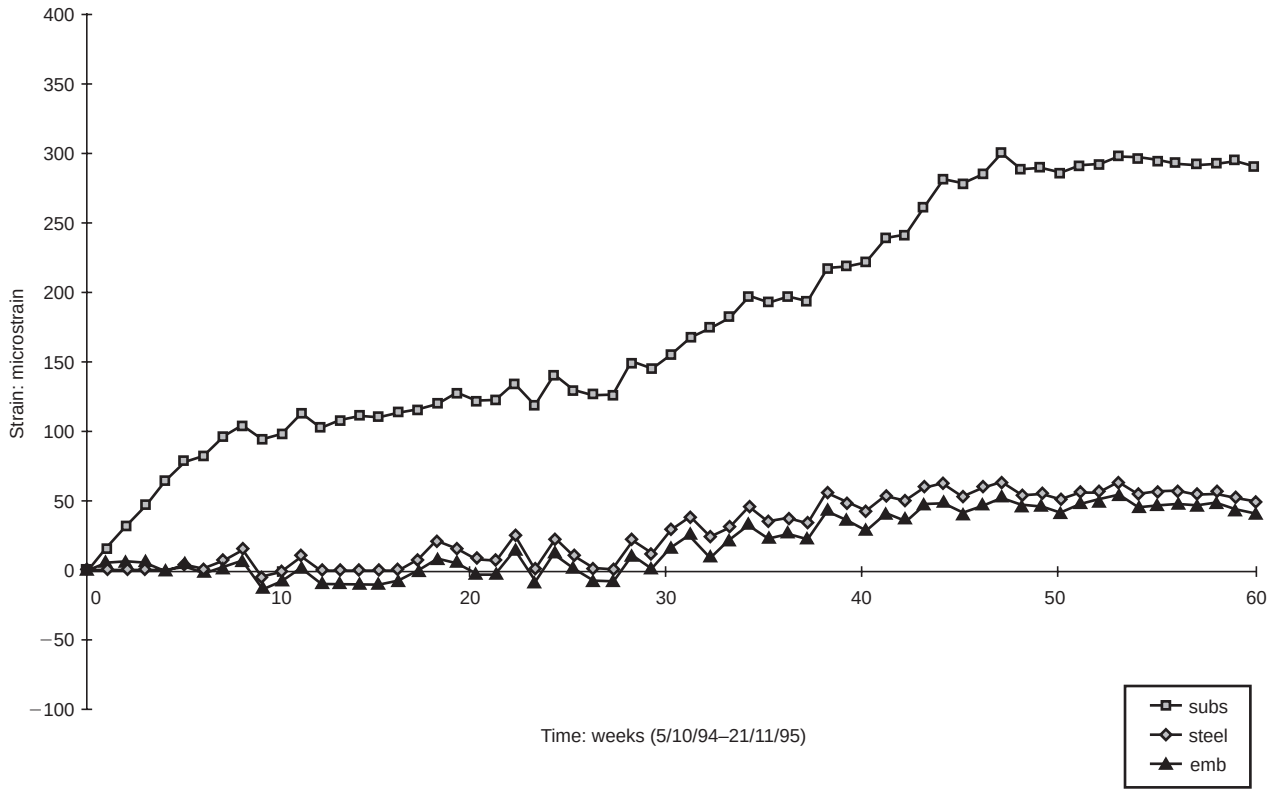

Fig. 4. Actual strain distribution in the repair patch of material L2 at Lawns Lane Bridge (tensile strain, negative; compressive strain, positive)

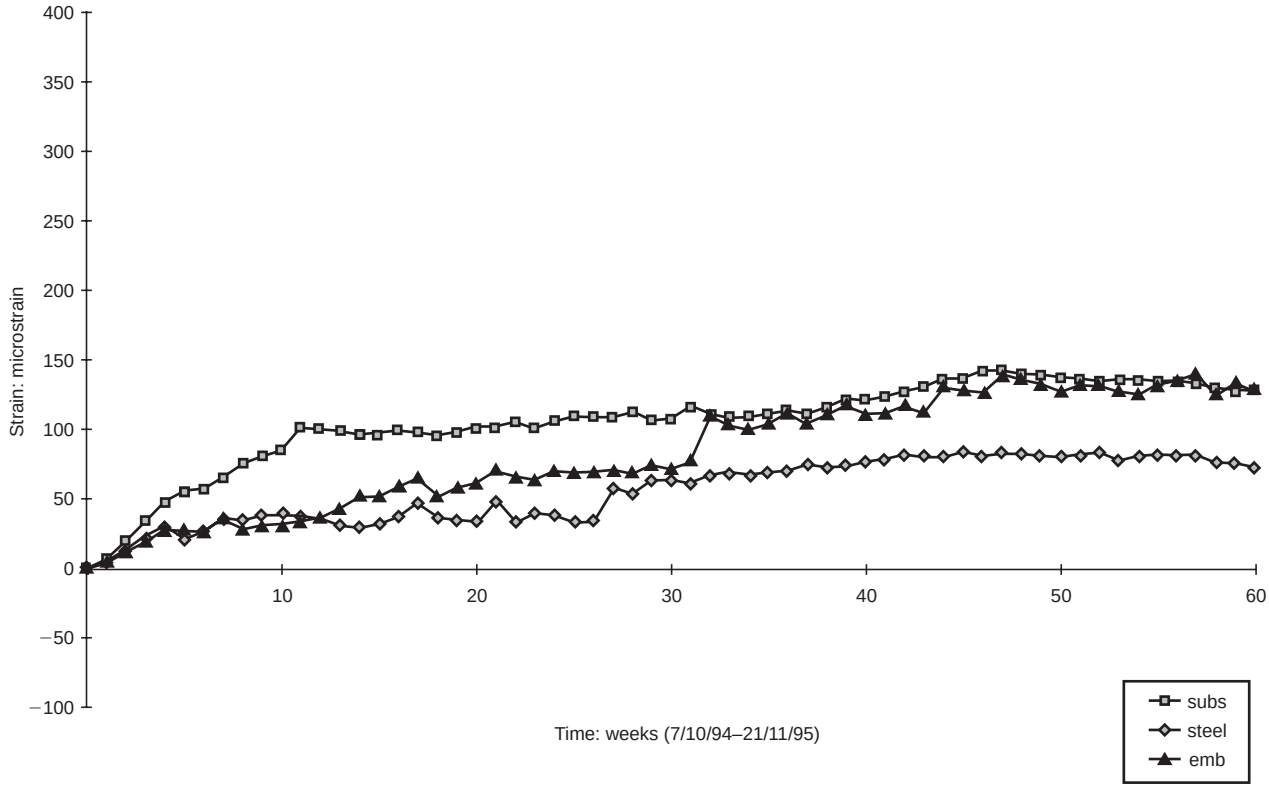

Fig. 5. Actual strain distribution in the repair patch of material L3 at Lawns Lane Bridge

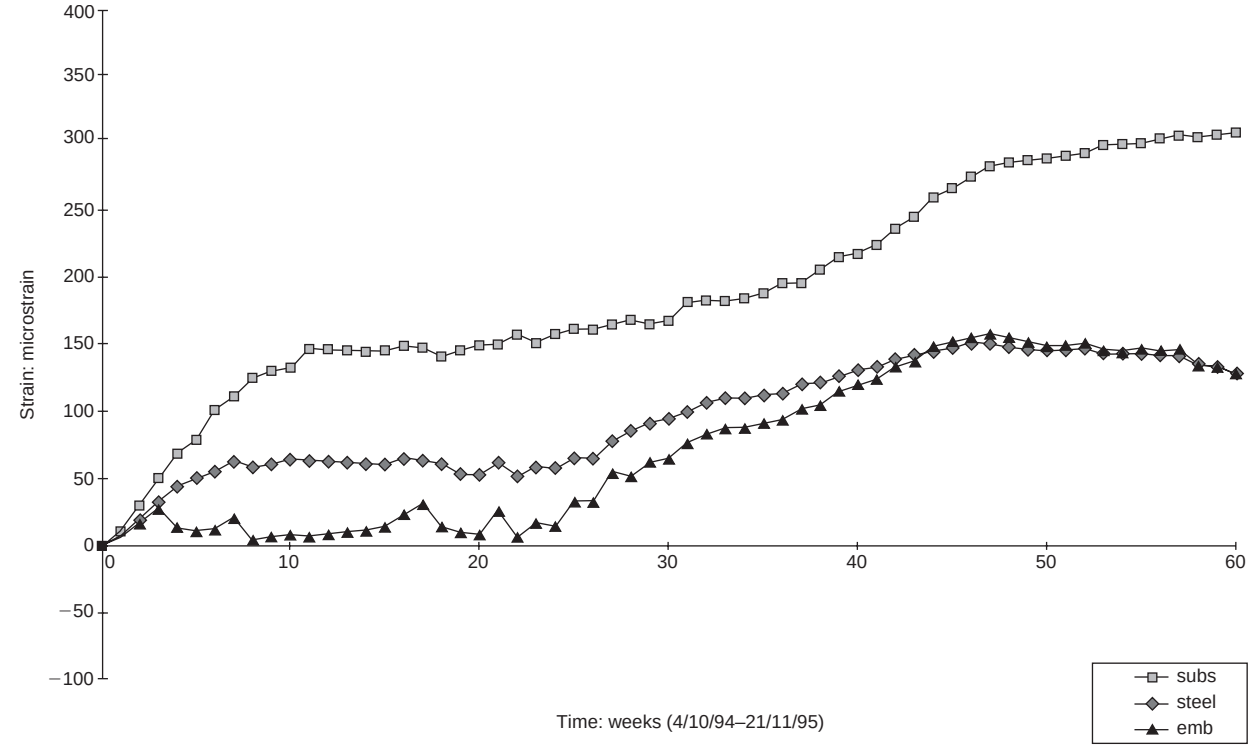

Fig. 6. Actual strain distribution in the repair patch of material L4 at Lawns Lane Bridge

25 weeks an increase in the substrate strain with time is again observed, until about week 47. From week 47 to the end of the monitoring period (week 60) the substrate strain remains relatively constant.

The strain profiles with time in the steel reinforcement ('steel' gauge) and within the repair material ('emb' gauge) during this period (weeks 0 to 60) are fairly similar to the profiles for the substrate concrete

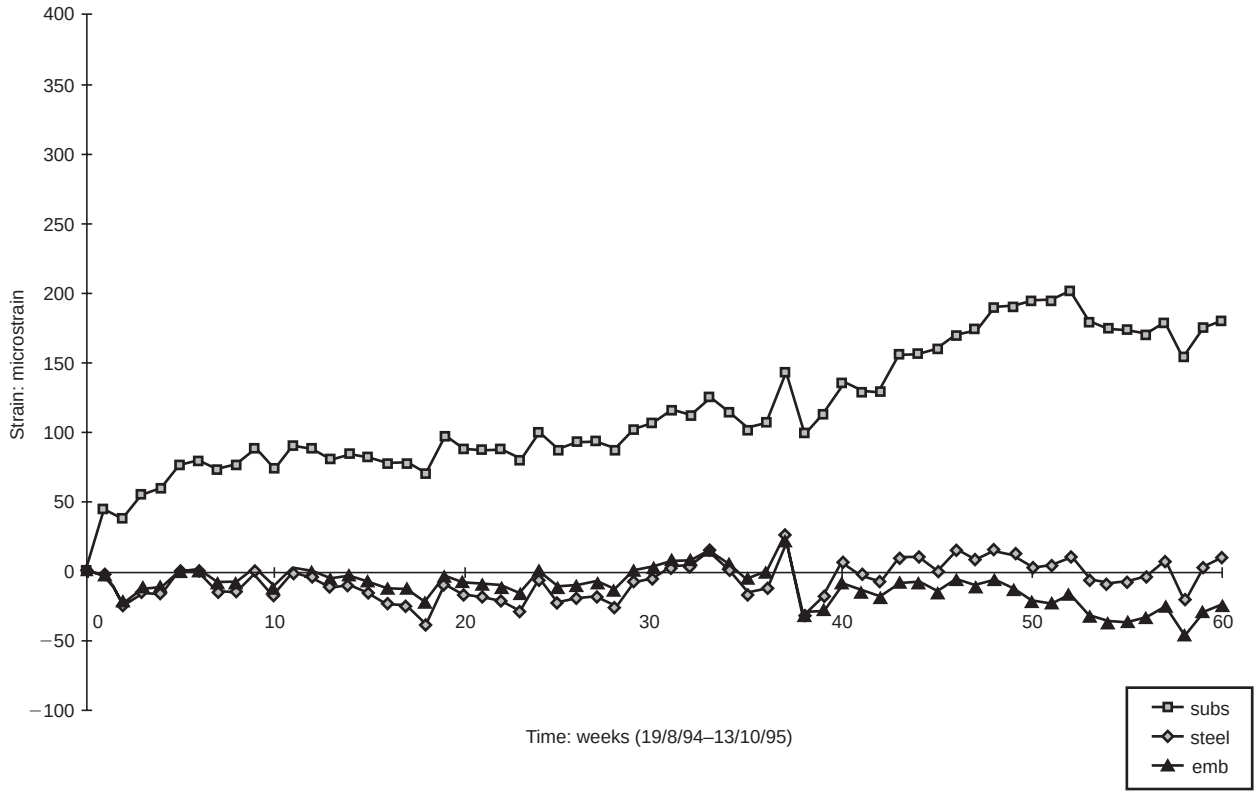

Fig. 7. Actual strain distribution in the repair patch of material G1 at Gunthorpe Bridge

but the magnitude of the strain is much lower in the steel and repair material than in the substrate interface. The repair patch at Gunthorpe Bridge with material G1 shows relatively constant strains in the steel and repair material during the monitoring period (Fig. 7). This is due to the fact that the dimensions of the abutment of Gunthorpe Bridge were extremely large (12·1 × 4·1 × 4·3 m) relative to the repair patches and, therefore, provided more effective restraint to the shrinkage of the repair material.

Period 0–11 weeks. The repair materials represented in Figs 4–7 have elastic moduli greater than those of the substrate concretes (see Table 1). As the stiffer repair materials exhibit shortening due to continuing shrinkage with time, compressive strain is transferred into the less stiff substrate. This results in an increasing compressive strain with time at the interface with the substrate concrete (weeks 0–11, Figs 4–7). This occurs after the repair material has hardened and attained an elastic modulus greater than that of the substrate. Most commercial repair materials are relatively rapidly hardening and attain over 95% of the 28 day elastic modulus in less than 20 days.[13] The large surface area of contact at the repair/substrate interface assists with the shrinkage strain transfer from the stiffer repair material to the substrate concrete. The rate of increase in the substrate strain is steep during weeks 0 to 11, when most of the shrinkage in the newly applied repair patch takes place. The maximum 'compressive' strain developed by the substrate at week 11 will be a function of the relative elastic moduli of the repair and substrate materials (the modular ratio) and of the free shrinkage and creep of the repair material. These properties are listed in Table 2. The relationship between the modular ratio E_{rm}/E_{sub} and the shrinkage strain transfer to the substrate is discussed further in a later section.

Compressive strain is also transferred by the shrinking repair material to the steel reinforcement during this period. However, the magnitude is much lower than the strain transferred to the substrate concrete, owing to the very high elastic modulus of the steel reinforcement. The steel reinforcement within the compression member lies in the same plane as the vibrating-wire gauge embedded in the repair material (gauge 'emb'). As a result, the longitudinal reinforcing bars which run adjacent to either side of the embedded gauge provide restraint to the shrinkage of the repair material. Consequently, the strains recorded by the 'emb' gauge are much lower than the free shrinkage of the repair materials (see below, Figs 8–11). The contraction strains of the repair material at the substrate interface level are greater than those at the steel reinforcement level ('emb' gauge level) since the restraint to shrinkage provided by the reinforcement decreases with increasing distance from the rebars. The restraint to shrinkage provided by the substrate concrete is low since $E_{rm} > E_{sub}$. The higher shrinkage of the repair material at the substrate interface level than at the 'emb' gauge

level results in the strains recorded by the 'subs' gauge being much greater than those recorded by the 'emb' gauge.

Period 11–60 weeks. After approximately 11 weeks the strain transfer to the substrate concrete reaches a stable state since shrinkage in the repair material has virtually ceased. This stable period lasts from week 11 to week 25 (Figs 4–7).

The next stage of redistribution of strain occurs from weeks 25 to 47, when external load is attracted from the substrate structure to the relatively stiffer repair patch. This results in gradually increasing strain with time both in the steel reinforcement within the repair patch and in the repair material. The strain compatibility between the repair material and the substrate at the interface also ensures an increasing strain at the substrate interface during this period. The external load transfer stage reaches a steady state at 47 weeks and a constant strain is maintained thereafter at the substrate interface and in the steel reinforcement.

Idealized distribution of strain

Figs 8–11 show simplified schematic distributions of strain with time for the repair patches of materials L2, L3, L4 and G1, respectively, based on the actual distributions of strain in Figs 4–7. The strains in the repair material ('emb' gauge) and the steel reinforcement ('steel' gauge) are averaged (owing to the assumed strain compatibility at the reinforcement level) and presented as single profiles in Figs 8–11.

The distributions of strain with time in Figs 8–11 are represented as a series of straight lines with four zones, namely Zone 1 (shrinkage transfer stage), Zone 2 (steady state 1), Zone 3 (external load transfer stage) and Zone 4 (steady state 2). The idealized zones identified in Figs 8–11 are based on field data monitored over 60 weeks in the piers and abutments of the two bridge structures (Lawns Lane and Gunthorpe bridges). Further monitoring will continue for some years. An update of the present findings will be given as long-term data become available, but initial indications are that the idealized zones identified in this paper are maintained and no new zones introduced. The zones identified in Figs 8–11 apply to materials with $E_{rm} > E_{sub}$. Repairs using materials with $E_{rm} < E_{sub}$ do not display these distinct zones, and shrinkage transfer (Zone 1) and external load transfer (Zone 3) do not occur in this case.[8] It is also possible that the idealized zones may vary between different structural elements and different bridge structures.

The cumulative strains obtained from Figs 8–11 at the end of each zone are listed in Table 3. Referring to Fig. 8 and Table 3, for repair material L2 the strain in the substrate concrete at the end of Zone 1 (week 11) is 120 microstrain. This strain is assumed to remain constant throughout Zone 2. The attraction of external load into the repair patch during Zone 3 increases the strain linearly to 300 microstrain at week 47. This strain remains constant thereafter as the repair patch and substrate concrete reach an equilibrium state. The strain in the steel reinforcement within the repair patch ('steel' gauge) and in the repair material between adjacent reinforcement bars ('emb' gauge) at the end of Zone 1 and during Zone 2 is 7 microstrain. This increases to 54 microstrain at the end of the external-load-transfer stage (Zone 3). Data for repair patches

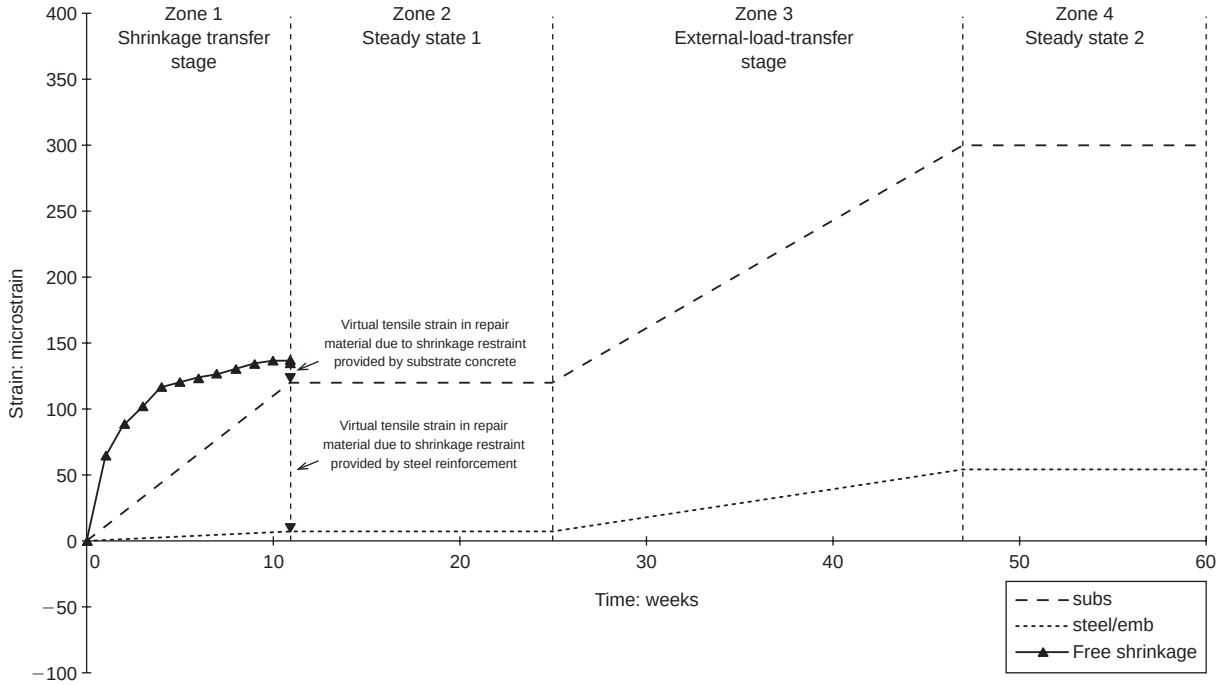

Fig. 8. Simplified distribution of strain in the repair patch of material L2 at Lawns Lane Bridge

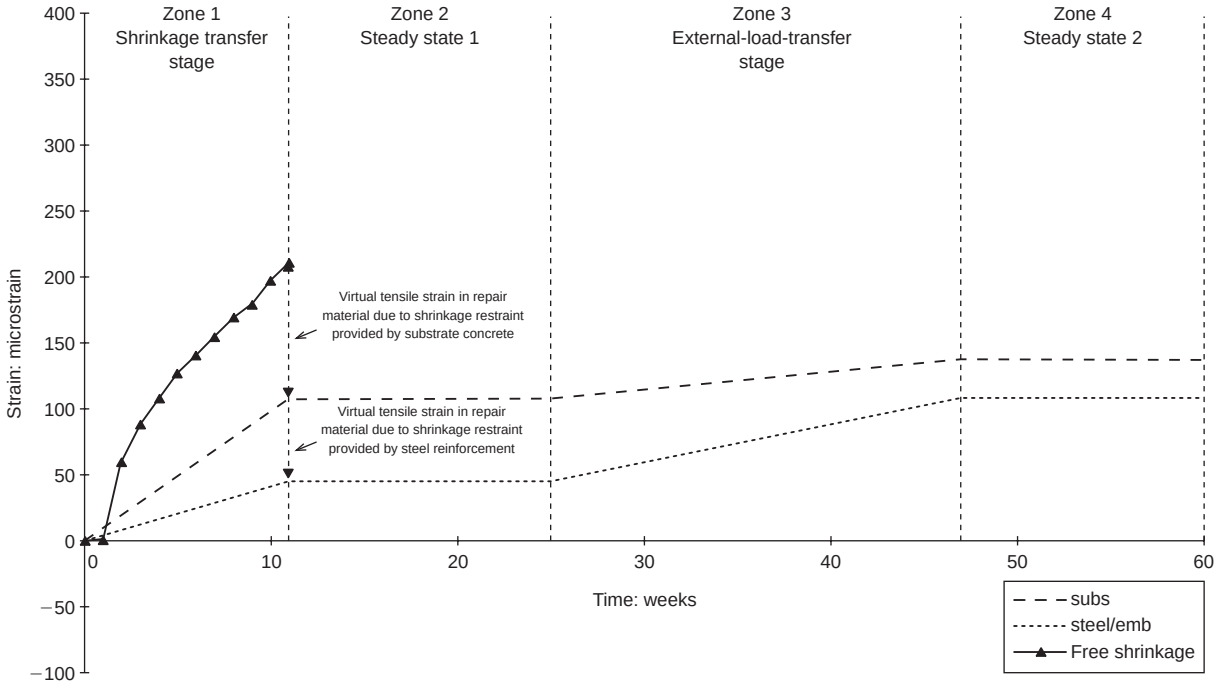

Fig. 9. Simplified distribution of strain in the repair patch of material L3 at Lawns Lane Bridge

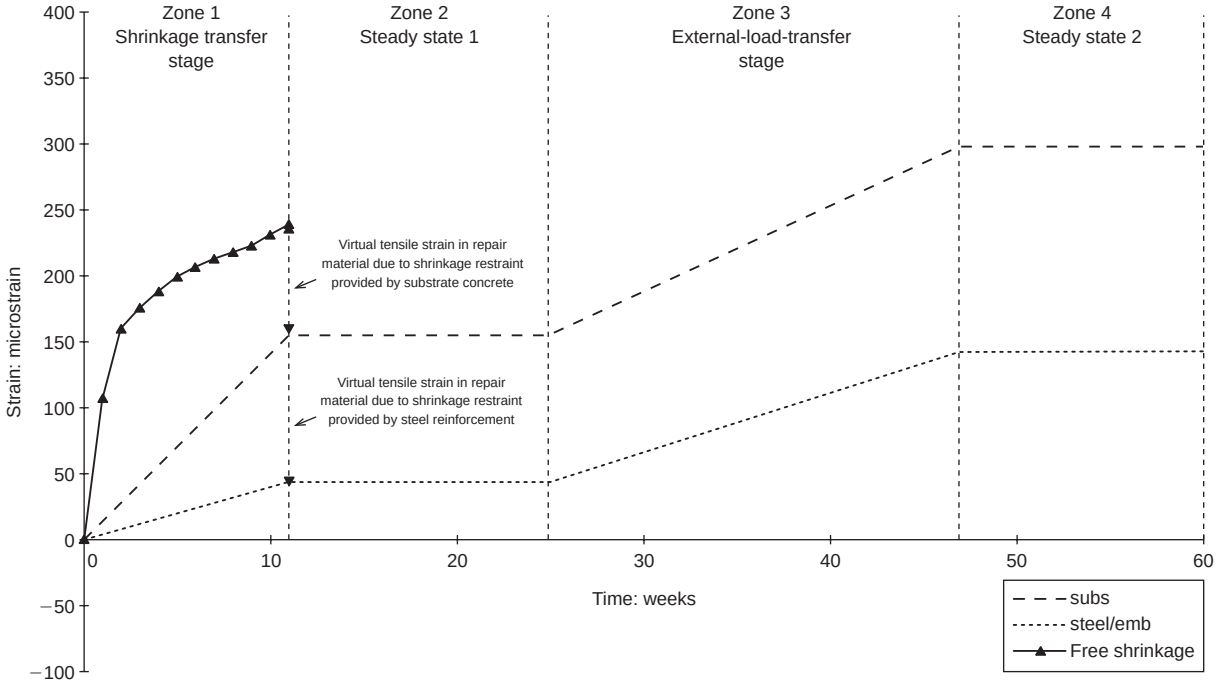

Fig. 10. Simplified distribution of strain in the repair patch of material L4 at Lawns Lane Bridge

made with the other materials are presented in a similar form in Table 3.

Influence of modular ratio (E_{rm}/E_{sub}) on shrinkage strain transfer to the substrate

The percentage of the free shrinkage strain of the repair material transferred to the substrate interface, λ, was calculated by dividing the strain $\epsilon_{sub(shr)}$ monitored at the substrate interface ('subs' gauge) at week 11 (end of shrinkage transfer stage) by the free shrinkage of the repair material $\epsilon_{shr(free)}$ at the same age. The values are given in Table 4. The free shrinkage of the repair materials $\epsilon_{shr(free)}$ was measured in the laboratory on $100 \times 100 \times 500$ mm size prisms which were stored at 20°C, 55% RH. The free shrinkage of the prisms at 100 days' age is given in Table 2, but in Table 4

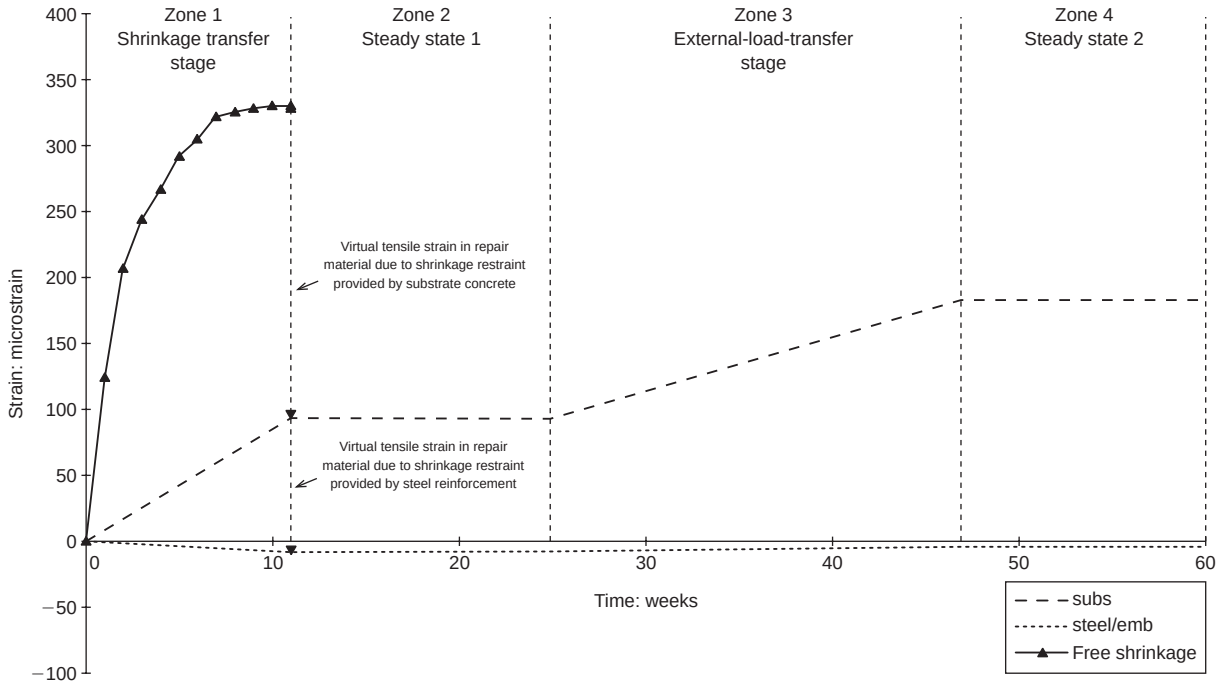

Fig. 11. Simplified distribution of strain in the repair patch of material G1 at Gunthorpe Bridge

Table 3. Cumulative strains developed in different stress transfer stages

Material	Location	Strain at end of: microstrain*			
		Zone 1 (week 11)	Zone 2 (week 25)	Zone 3 (week 47)	Zone 4 (week 60)
L2	'subs'	+120	+120	+300	+300
	'steel'/'emb'	+7	+7	+54	+54
L3	'subs'	+107	+107	+137	+137
	'steel'/'emb'	+45	+45	+108	+108
L4	'subs'	+154	+154	+297	+297
	'steel'/'emb'	+42	+42	+142	+142
G1	'subs'	+92	+92	+183	+183
	'steel'/'emb'	−9	−9	−4	−4

* Negative values indicate tensile strains.

Table 4. Percentage of shrinkage strain of repair transferred to the substrate concrete, λ

Repair material	m (E_{rm}/E_{sub})	$\varepsilon_{sub(shr)}$: microstrain	$\varepsilon_{shr(free)}$: microstrain	λ: %
L2	1·27	120	136	88
L3	1·15	107	210	51
L4	1·22	154	238	65
G1	1·10	92	329	28

correction factors have been applied[14] to account for the difference between laboratory and field conditions (i.e. volume/surface ratio, temperature and humidity) as outlined later.

The modular ratio m (E_{rm}/E_{sub}) is also given in Table 4 for the repair patches incorporating materials L2, L3 and L4 (Lawns Lane Bridge) and G1 (Gunthorpe Bridge). A graph of m versus λ is plotted in Fig. 12, which shows a linear relationship with a coefficient of correlation of 0·97. The best-fit equation is

$$m = 0{\cdot}0032\,\lambda + 1 \tag{2}$$

Rearranging equation (2) gives

$$\lambda = \frac{m - 1}{0{\cdot}0032} \tag{3}$$

The range of experimental data in Fig. 12 which is represented by equations (2) and (3) falls within the limits $28 \leqslant \lambda \leqslant 88$.

The value of m (from equation (3)) which yields the lower limit of $\lambda = 28\%$ is 1·1 (Fig. 12). The low degree of shrinkage transferred to the substrate (λ) at $m < 1{\cdot}1$ will result in higher restrained-shrinkage tension at the interface and consequently a greater risk of cracking in the repair. At the upper limit of $\lambda = 88\%$ represented by the experimental data in Fig. 12, the value of m (from equation (3)) is 1·3. The free shrinkage transferred to the substrate (λ) approaches 100% as m exceeds 1·3. Therefore, the use of a relatively high-stiffness repair material with $m > 1{\cdot}3$ will ensure a very high degree of free-shrinkage transfer to the substrate. For example, the elastic modulus of the substrate concrete at Lawns Lane Bridge is 23·8 kN/mm^2. Therefore, a repair material with an elastic modulus $E_{rm} > 23{\cdot}8 \times 1{\cdot}3$ (i.e. 31 kN/mm^2) would transfer most of its free shrinkage to the substrate concrete. As a result, the repair at the interface will develop negligible tension and cracking will not be a problem.

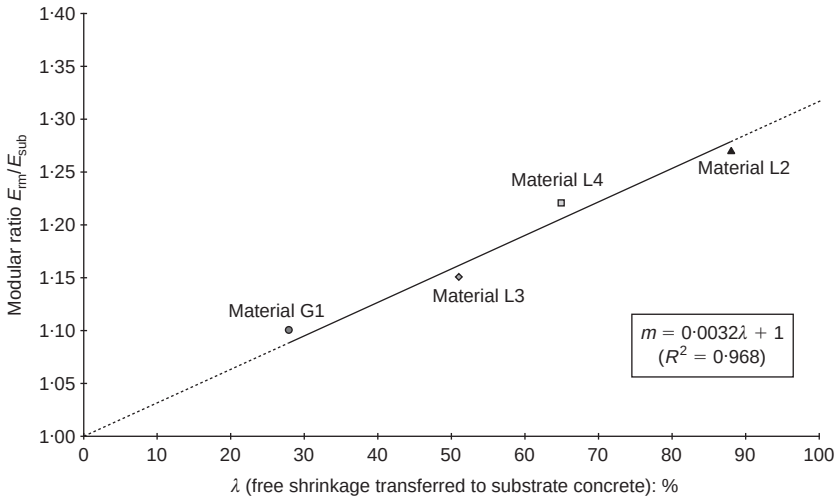

Fig. 12. Relationship between modular ratio ($E_{rm}/E_{sub} = m$) and percentage of free shrinkage transferred to the substrate concrete

Tension in repair material due to restrained shrinkage

The free shrinkage of the repair material in the repair patch, from week 0 to week 11, is plotted in Figs 8–11 along with the idealized strain distribution profiles of materials L2, L3 and L4 (Lawns Lane Bridge) and G1 (Gunthorpe Bridge). The free-shrinkage data obtained in the laboratory have been modified by applying correction factors (for volume/surface ratio, temperature and humidity) to plot the free-shrinkage graphs in Figs 8–11.[14] The prism specimens ($100 \times 100 \times 500$ mm) tested in the laboratory have a different volume/surface ratio from the field repair patch. A higher volume/surface ratio will contribute to lower shrinkage in the repair patch and vice versa. Similarly, differences in the laboratory temperature and humidity from the field conditions will result in variations in shrinkage between the repair patches and laboratory specimens. The nonlinear relationship between relative shrinkage and volume/surface ratio given by Kong and Evans[14] was used to assess the shrinkage in the repair patch on the basis of data obtained from laboratory specimens at 55% RH. The relative humidity for the field concrete was consistently higher—at early ages the patch repairs were cured under covered conditions, which resulted in particularly high humidity. The correction for RH differences was applied as follows:[14] 2% decrease in shrinkage for each 1% increase in RH to 70%; 3% decrease in shrinkage for each 1% increase in RH from 70% to 90%. The temperature correction was applied on the basis of a 1% decrease in shrinkage for each degree Celsius fall in temperature.[14] The repair patch temperature over the eleven-week shrinkage period had an average value of 10°C.

The magnitude of virtual tensile strain in the repair material due to the shrinkage restraint provided by the substrate concrete (at the interface) and the steel reinforcement is also shown in Figs 8–11. The values are listed in Table 5. The virtual tensile strain causes tensile stress in the repair material at the substrate/repair and reinforcement/repair interfaces. The tension in Figs 8–11 (and Table 5) was determined as the difference between the free shrinkage of the repair material and the compressive (shrinkage transfer) strain in either the substrate concrete or the steel reinforcement. For example, the free shrinkage at week 11 of material L4 is 238 microstrain (Table 5). The strains monitored at the substrate interface and in the steel reinforcement at week 11 were 154 and 42 microstrain, respectively. This gives virtual tensile strains in the repair material of 84 and 196 microstrain at the interfaces with the substrate and reinforcement, respectively. The corresponding tensile stress in the repair material was determined by multiplying with the elastic modulus (Table 5).

The tensile stress at the interface increases incrementally with continuing shrinkage of the repair material. This tensile stress will lead to tensile creep and a consequent relaxation of the tensile stress. The degree of relaxation will depend on the creep property of the repair material (Table 2) and the applied stress/strength ratio. The tensile stresses shown in Table 5 are quite high (in most cases) and, therefore, result in a high stress/strength ratio and consequently high relaxation due to creep. The tensile stresses listed in Table 5 are only indicative values which represent the effect of cumulative shrinkage at week 11. In reality, relaxation due to incremental creep would occur continuously, owing to gradually increasing shrinkage strain. In addition, any slip at the interface before the repair material had fully hardened is not taken into account when calculating the tensile stresses. Consequently the actual tensile stresses in the repair patch are expected to be significantly lower than the values listed in Table 5.

Material L3 has particularly high creep characteristics (Table 2) and, therefore, undergoes very high relaxation due to creep. This is verified by Fig. 9, for

Table 5. Tensile strain (virtual) and stress in the repair material due to restrained shrinkage

Bridge	Material	Free shrinkage at week 11: microstrain*	Elastic modulus E_{rm}: kN/mm^2	Location	Strain at week 11: microstrain	Strain (virtual): microstrain†	Tensile stress: N/mm^2†
Lawns Lane	L2	136	30·3	'subs'	120	−16	0·5
				'steel'/'emb'	7	−129	3·9
	L3	210	27·4	'subs'	107	−103	2·8
				'steel'/'emb'	45	−165	4·5
	L4	238	29·1	'subs'	154	−84	2·4
				'steel'/'emb'	42	−196	5·7
Gunthorpe	G1	329	31·1	'subs'	92	−237	7·4
				'steel'/'emb'	−9	−338	10·5

* Modified by applying correction factors for volume/surface ratio, temperature and humidity differences between the field repair patch and laboratory test data.[14]

† Due to restrained shrinkage of the repair material at the substrate interface and at the reinforcement interface.

material L3, which shows lower transfer of strain to the substrate between weeks 11 and 60 compared with the other repairs represented in Figs 8–11. Sufficiently high levels of creep can ultimately reduce the effective modulus of elasticity of the repair material to less than E_{sub}, thereby rendering it ineffective for shrinkage transfer to the substrate.

The tensile stresses due to restrained shrinkage listed in Table 5 are much higher at the reinforcement interface. This suggests that the risk of tensile cracking initiating at the reinforcement surface is much greater than at the substrate interface. Table 5 also shows that the tensile stresses induced in material G1 at Gunthorpe Bridge are by far the greatest. This again confirms the very high restraint provided by the abutment at Gunthorpe Bridge to the small-size repair patch.

All the repair materials represented in Figs 8–11 (and in Table 5) performed well under service conditions during the 60 week monitoring period and *no* cracking was observed in the repair patches of these materials.

Schematic representation of strain redistribution with time

A schematic representation of the long-term strain redistribution in the repair and substrate materials of a repaired compression member is given in Fig. 13, on the basis of the observations from the experimental results. A repair material with an elastic modulus E_{rm} greater than that of the substrate (E_{sub}) is considered. The effect of steel reinforcement is omitted for simplicity and to aid clarity. Fig. 13(a) shows a cross-section through an unpropped compression member before the deteriorated patch was removed. Fig. 13(b) shows the same section after the removal of the deteriorated patch. Fig. 13(c) shows the cross-section after the application of the repair (weeks 0 to 11, shrinkage transfer stage).

Shrinkage transfer stage (weeks 0 to 11, Zone 1). During weeks 0 to 11, the stiffer repair material ($E_{rm} > E_{sub}$) shrinks incrementally and transfers a proportion of its shrinkage strain to the substrate concrete. The resulting idealized distribution of strain (on an exaggerated scale) is shown in Fig. 13(d). Strain compatibility at the substrate/repair interface is maintained and the strains towards the free face of the repair gradually increase owing to decreasing restraint by the substrate. The strain profile described above is not entirely compatible with the data plotted in Figs 4–7, owing to the omission of the steel reinforcement in the schematic representation (Fig. 13) for the sake of simplification. Inclusion of the steel reinforcement and taking account of its restraint to the shrinkage of the repair material in its vicinity provides satisfactory agreement between the field data (Figs 4–7) and the schematic representation (Fig. 13(d)). The shrinking repair material with $E_{rm} > E_{sub}$ will deform a zone of the substrate in the proximity of the interface (Fig. 13(d), 'zone of influence'). The resulting compressive strain will be maximum at the substrate interface and gradually reduce to zero at the end of the 'zone of influence'. The shrinkage transfer to the substrate will result in low compressive stress relative to the compressive strength of the substrate. For example, the monitored strain at the substrate interface at week 11 for the patch repair with material L4 (Fig. 10, Table 3) is 154 microstrain. A value of $E_{sub} = 23{\cdot}8$ kN/mm^2 at Lawns Lane Bridge gives a compressive stress in the substrate (interface) of 3·67 N/mm^2. The compressive strength of the substrate concrete was 42 N/mm^2.

The restraint to the free shrinkage of the repair provided by the substrate will result in maximum tensile stress in the repair material at the interface, reducing gradually towards the free face of the repair patch

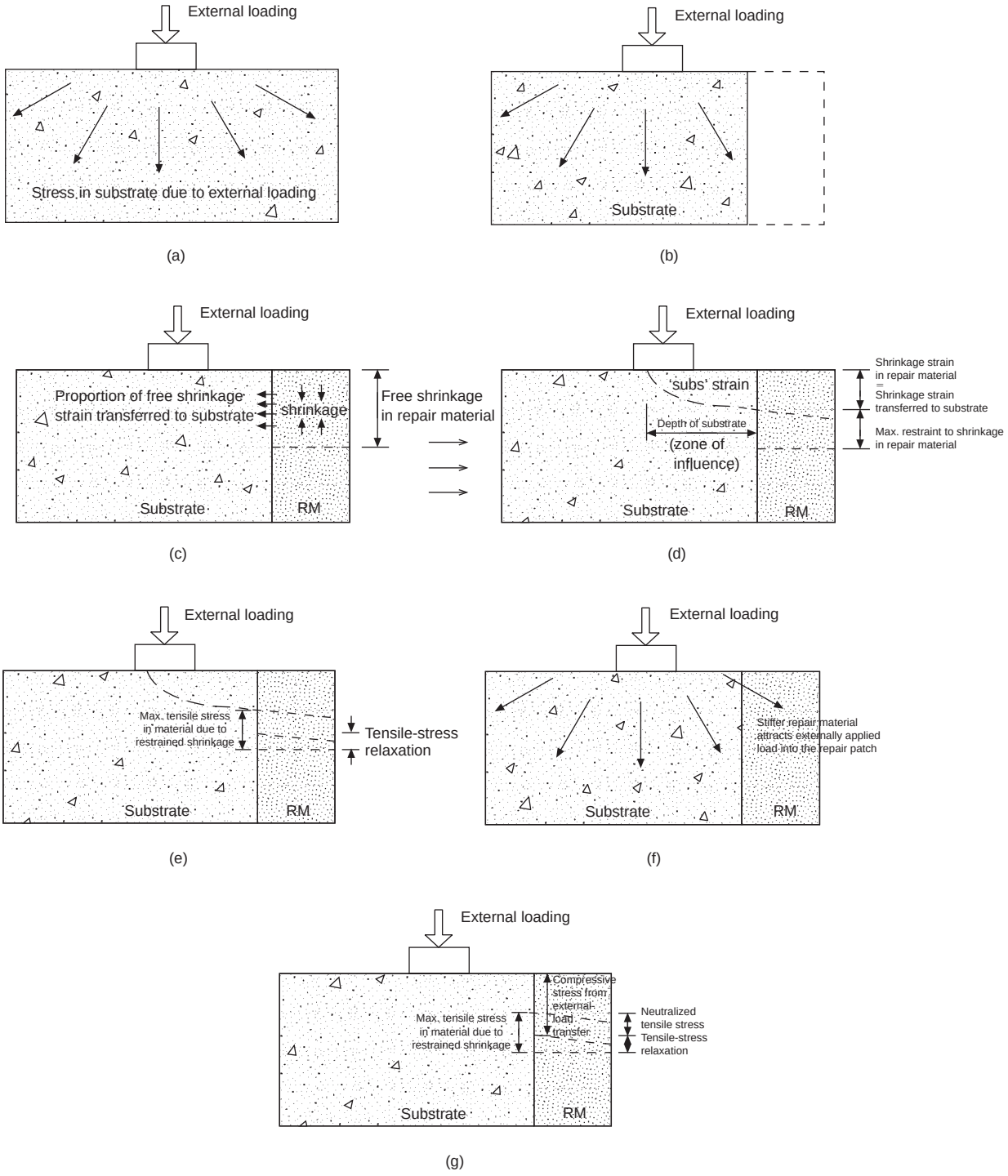

Fig. 13. Schematic redistribution of shrinkage and external-load-transfer strains to the repair patch of a compression member ($E_{rm} > E_{sub}$) (RM, repair material): (a) section through substrate before deteriorated concrete removed; (b) section through substrate after deteriorated concrete removed; (c) repair material applied and shrinkage takes place (weeks 0 to 11); (d) idealized redistribution of shrinkage strain (weeks 0 to 11); (e) repair material undergoes tensile creep resulting in stress relaxation (weeks 0 to 11); (f) repair material stabilizes after shrinkage and creep (weeks 11 to 25) and attracts externally applied load (weeks 25 to 47); (g) idealized transfer of external compression from substrate which neutralizes tensile stress in repair material (weeks 25 to 47)

(Fig. 13(d)). The tensile stress leads to creep and consequent relaxation of the tensile stress (Fig. 13(e)).

External-load-transfer stage (weeks 25 to 47, Zone 3). Figure 13(f) shows that the externally applied load to the structural member is attracted into the repair patch at the end of the steady-state period (week 25). This transfer may, in due course, neutralize the residual tensile stress in the repair material

caused by restrained shrinkage, as shown in Fig. 13(g). The strain compatibility at the repair/substrate interface during the load transfer stage means that a measure of the load transferred to the repair interface can be estimated from the difference between the 'subs' vibrating-wire gauge readings between weeks 25 and 47. These values were calculated from the data listed in Table 3 and are given in Table 6. It is clear from Table 6 that a higher modular ratio results in greater external-load (strain) transfer into the repair patch. Material L3 is an exception to this observation owing to its very high creep characteristics.

The structural members of the bridges were repaired in an unpropped state and, therefore, the external loading was similar during and after repair. The fact that, in the long term, load transfer occurs from the substrate to the repair patch (without any change in external loading) is a significant finding of this research and is due to stress redistribution occurring as composite action between the repair reinforcement and substrate is consolidated in the long term. Efficient composite action is facilitated by good bond at the repair interface and by the continuity provided by the steel reinforcement which penetrates both the substrate and the repair patch. The thickness of repair (140 mm) used is sufficiently large to provide adequate embedment to the reinforcement and, therefore, result in continuity and load sharing with the substrate. Basic composite mechanics shows that repair materials with $E_{rm} > E_{sub}$ are more effective in attracting load from the substrate. Rigorous theoretical analyses of the problem have been carried out[15] to quantify the load transfer to the repair patch. Repair patches with $E_{rm} < E_{sub}$ do not show effective external-load transfer from the substrate to the repair.[8]

Recommendations for selection of repair materials

The results presented in this paper show that the basic repair material properties of elastic modulus, shrinkage and creep have a dominant effect on the in-service performance of a concrete repair. Satisfactory bond between the repair and substrate is, of course, a fundamental prerequisite to satisfactory performance. The compressive strength of a repair material is relatively unimportant. Current standards for repair material specifications such as BD27/86[1] and current knowledge on the subject[16–18] lack adequate appreciation of these factors. For example, the repair materials L2, L3 and L4 did not conform to the repair standard BD27/86[1] but, nevertheless, performed perfectly satisfactorily over the 60 week monitoring period. Current practice for repair tends to recommend higher strength of the repair material relative to the substrate, similar elastic moduli of the two materials ($E_{rm} \sim E_{sub}$) and lower shrinkage of the repair material.[16–18] The findings of this research, however, show that if $E_{rm} \sim E_{sub}$ (i.e. $m = 1$), the repair material is unable to transfer shrinkage strains to the substrate concrete. This will induce relatively high tensile stress in the repair material owing to restrained shrinkage, thereby increasing the potential for cracking. The long-term transfer of external load to the repair patch will also be ineffective if $E_{rm} \leqslant E_{sub}$. For optimum performance of the repair it is important that E_{rm} is considerably greater than E_{sub}. It is also meaningless to recommend that the shrinkage or creep of a repair material should bear any relationship to the substrate.[16–18] The substrate concrete in structures which undergo repair is usually quite old and has attained dimensional stability, whereas the repair material is new. For example, Gunthorpe Bridge, monitored in this project, has been in service for 68 years.

Table 6. Strain induced in the repair material (at interface) due to external-load transfer (weeks 25 to 47)

Repair material	m	$\epsilon_{\text{load transfer}}$: microstrain*
L2	1·27	180
L3	1·15	30†
L4	1·22	143
G1	1·10	91

* $\epsilon_{\text{load transfer}} = \epsilon_{\text{'subs' week 47}} - \epsilon_{\text{'subs' week 25}}$ (from Table 3).
† Low external-load-transfer strain due to very high creep of material L3.

Conclusions

The following conclusions are based on the results of the in-service monitoring of repairs applied to two highway bridges.

(*a*) There are four stages of strain (and consequently stress) redistribution in spray-applied repair patches (with $E_{rm} > E_{sub}$) to unpropped compression members:
  (i) a shrinkage transfer stage (weeks 0 to 11)
  (ii) steady state 1 (weeks 11 to 25)
  (iii) an external-load-transfer stage (weeks 25 to 47)
  (iv) steady state 2 (weeks 47 to 60).

(*b*) A repair material which has a greater elastic modulus than the substrate concrete ($E_{rm} > E_{sub}$) is able to transfer a proportion of its shrinkage strain to the substrate concrete. This reduces the restrained-shrinkage tension in the repair and consequently reduces the risk of cracking.

(*c*) An optimum choice of $E_{rm} > 1{\cdot}3E_{sub}$ is recommended from the field data to ensure a high level of free-shrinkage transfer to the substrate (> 88%), thereby reducing the risk of restrained-shrinkage cracking to negligible levels.

(*d*) A repair material with $E_{rm} > E_{sub}$, applied to a compression member, will attract externally applied load into the repair patch in the long term.

(*e*) Relatively low creep characteristics of repair ma-

terials are desirable to ensure that E_{rm} remains greater than E_{sub} so that effective redistribution of external load to the repair patch can take place in the long term.

(*f*) Current standards for repair material specifications, e.g. BD27/86 of the Highways Agency, have significant limitations.

Acknowledgements

This paper is based on a LINK TIO-funded project entitled 'Long-term performance of concrete repair in highway structures'. The partners in the project were Sheffield Hallam University, V A Crookes (Contracts) Ltd, Flexcrete Ltd, M. J. Gleeson Group plc and the Department of Transport.

References

1. Department of Transport. *Materials for the Repair of Concrete Highway Structures.* DoT, London, 1986, BD27/86.
2. Emmons P. H. and Vaysburd A. M. *Performance Criteria for Concrete Repair Materials, Phase 1*. US Army Corps of Engineers, Technical Report, in press.
3. Emmons P. H. and Vaysburd A. M. A total system concept—necessary for improving the performance of repaired structures. *Concrete International*, 1995, Mar., 31–36.
4. Mangat P. S. and Limbachiya M. K. Repair materials properties which influence long-term performance of concrete structures. *Construction and Building Materials*, 1995, **9**, No. 2, 81–90.
5. Mangat P. S. and Limbachiya M. K. Repair material properties for effective structural application. *Cement and Concrete Research*, 1997, **27**, No. 4, 601–617.
6. Mangat P. S. and O'Flaherty F. J. Long-term performance criteria for concrete repair materials. Keynote paper. *International Congress on Creating with Concrete*. Dundee, 1999.
7. Emberson N. K. and Mays G. C. Significance of property mismatch in the patch repair of concrete. Part 3: reinforced concrete members in flexure. *Magazine of Concrete Research*, 1996, **48**, No. 174, 45–57.
8. Mangat P. S. and O'Flaherty F. J. Influence of elastic modulus on stress redistribution and cracking in repair patches. *Cement and Concrete Research*, in press.
9. Plum D. R. Repair materials and repaired structures in a varying environment. *Proceedings of the 3rd International Seminar on the Life of Structures—the Role of Physical Testing, Brighton*, 1989, 77–84.
10. Rizzo E. M. and Sobelman M. B. Selection criteria for concrete repair materials. *Concrete International*, 1989, Sept., 46–49.
11. British Standards Institution. *Method for Determination of Static Modulus of Elasticity in Compression*. BSI, Milton Keynes, 1983, BS 1881: Part 121.
12. British Standards Institution. *Method for Determination of Compressive Strength of Concrete Cubes.* BSI, Milton Keynes. 1983, BS 1881: Part 116.
13. Pinelle D. J. Curing stresses in polymer modified repair mortars. *Cement, Concrete and Aggregates*, CCAGDP, 1995, **17**, No. 2, 195–200.
14. Kong F. K. and Evans R. H. *Reinforced and Prestressed Concrete*. Van Nostrand Reinhold, 3rd edn, Wokingham, 1987.
15. O'Flaherty F. J. *Long Term Performance of Concrete Repair in Highway Structures.* PhD thesis, Sheffield Hallam University, 1998.
16. Dector M. H. and Lambe R. W. New materials for concrete repair—development and testing. *Indian Concrete Journal*, 1993, Oct., 475–480.
17. Emberson N. K. and Mays G. C. Significance of property mismatch in the patch repair of structural concrete. Part 1: properties of the repair system. *Magazine of Concrete Research*, 1990, **42**, No. 152, 147–160.
18. Wood J. G. M., King E. S. and Leek D. S. Defining the properties of concrete repair materials for effective structural application. *International Conference on Structural Faults and Repair-89.* London, 1989, p. 2.

Discussion contributions on this paper should reach the editor by 31 March 2000